THE ASTROPHYSICAL JOURNAL, 357:140–148, 1990 July 1

THE EVOLUTIONARY SEQUENCE OF PLANETARY NEBULAE

M. A. DOPITA AND S. J. MEATHERINGHAM[1]
Mount Stromlo and Siding Spring Observatories, Australian National University
Received 1989 August 28; accepted 1989 December 20

ABSTRACT

We develop a simple model for the evolution of planetary nebulae (PNs) using the large and homogeneous data set accumulated in recent times on the Magellanic Cloud PN population. In this model, a high-velocity radiation pressure driven wind interacts with the dense un-ionized shell of material ejected during the asymptotic giant branch evolution. This wind serves to confine by ram pressure the ionized gas and to accelerate the nebula. During the optically thin period, the nebulae fade at almost constant expansion velocity. Higher mass planetary nebulae nuclei (PNN) accelerate their associated nebulae to higher velocities. This model reproduces the observed density-radius–ionized mass–dynamical age relationships and serves to define the geometrical relationship between the ionized nebula and the central star.

Using a grid of model atmospheres, we have generated theoretical evolutionary tracks on the excitation class versus Hβ flux plane, which we show to be a form of the log $T_{\rm eff}$ versus log $(L/L_\odot)$plane (Hertzsprung-Russell diagram) transformed to explicit coordinates of the nebular parameters. A comparison of these tracks with the observed points demonstrates that the PNN in the Magellanic Clouds are confined in the mass range 0.55–0.7 $M_\odot$, with a peak at $\sim$0.64 $M_\odot$.

Finally, we have used photoionization models computed along the evolutionary tracks to show that secondary line ratios used to define the excitation class are also correctly predicted, and we present evidence that the third dredge-up episode appears to have enhanced both He and N in the more massive PNs in the LMC.

Subject headings: nebulae: planetary — stars: evolution — stars: winds

I. INTRODUCTION

Considerable progress has been made in our understanding of the details of planetary nebula evolution since the pioneering work of Harman and Seaton (1964). It has become clear that the original Harman-Seaton sequence is in fact the superposition of several different mass tracks of the planetary nebula nuclei (PNN) in the range 0.6–1.2 $M_\odot$ (Paczyński 1971; O'Dell 1974; Pottasch 1984). Evolutionary calculations of the central stars have been carried through by a number of authors (Härm and Schwartzschild 1975; Schönberner 1979, 1981, 1983; Iben 1984; Wood and Faulkner 1986). These models emphasize the great sensitivity of the tracks on the Hertzsprung-Russell diagram to the details of the helium shell flash phase and to the mass loss from the central star.

Dynamical models for the evolution of the nebula itself have been constructed by several authors (Mathews 1966; Sofia and Hunter 1968; Kwok, Purton, and Fitzgerald 1978; Kwok 1982). It is clear that the ionized nebula evolves in the material ejected by the asymptotic giant branch (AGB) precursor star. What is not so clear is whether this material is ejected in a slow wind or in a much more sudden "superwind" episode (Wood and Cahn 1977; Kwok, Purton, and Fitzgerald 1978). In each case, the dynamical evolution of the subsequent nebula would be quite different (Kwok 1982; Sabbadin *et al.* 1984).

As the central star evolves toward the blue, a fast stellar wind, presumably radiation pressure driven, compresses and accelerates the partially ionized preejected material, confining it to a thin shell. According to Phillips (1984), the ionized shell has a fractional thickness of $\Delta R/R \sim 0.1$–0.15, with little dependence on the radius of the nebula. This result agrees well with what has been inferred dynamically (Dopita *et al.* 1988; Meatheringham, Wood, and Faulkner 1988).

[1] Currently at NASA Goddard Space Flight Center.

The photoionization evolution of the nebula is currently very poorly understood. For a few individual nebulae, very sophisticated models have been constructed (e.g., Harrington *et al.* 1982; Clegg *et al.* 1986). However, evolutionary models have often been rather simplified and empirical and are not fully consistent with what is known about the dynamical evolution (Kaler 1978, 1980; Sabbadin 1986). Exceptions are to be found in the work of Vil'koviskii, Kondat'eva, and Tamovtseva (1983), Okorokov *et al.* (1985), Schmidt-Voigt and Köppen (1987*a*, *b*), and Stasinska (1989), who all take into account the evolution of the central star and the expansion of the envelope.

During the past few years, we have accumulated a considerable body of homogeneous data on the diameters, fluxes, expansion velocities, and kinematics of the population of planetary nebulae (PNs) in the Magellanic Clouds (Dopita *et al.* 1985, 1987, 1988; Dopita, Ford, and Webster 1985; Meatheringham *et al.* 1988; Meatheringham, Dopita, and Morgan 1988; Wood, Bessell, and Dopita 1986; Wood *et al.* 1987). This sample has the advantage of being at a common and known distance, of having low reddening, and of being close enough for detailed study. The long-term objective of this work has been to attempt to achieve an understanding of the process of PN ejection and of the post–AGB evolution of the central star as it evolves into a white dwarf.

In principle, given the uncertainties in the processes of mass ejection from the central star and its subsequent evolution, it is possible to conceive that there could be little correlation between the nebular parameters and those of the central star. The importance of our work (Dopita *et al.* 1987, 1988) has been to establish observationally that the parameters of a planetary nebula are in fact uniquely determined by the parameters of the central star. Thus, studies of the nebula will define the evolution of the central star, even in cases in which the central star cannot be observed directly.

In this paper we present a first-order solution to the problem of nebular evolution, which in turn allows us to construct photoionization models with the correct geometry of the ionized gas with respect to the central star. We use these to investigate the evolution of the central star in terms of a "transformed" H-R diagram, in which Hβ luminosity replaces stellar luminosity and the nebular excitation class takes the place of stellar effective temperature.

II. THE OBSERVATIONAL DATA BASE

The sample of PNs that we have observed is drawn from the catalogs of Sanduleak, MacConnell, and Philip (1978), Jacoby (1980), and Morgan and Good (1985). The first is a complete sample down to a flux limit of about log $F_{\mathrm{H}\beta} \sim -13.3$ ergs cm^{-2} s^{-1}, the second is a complete sample to a much fainter limiting magnitude in [O III], but covering only a restricted region of the Clouds, and the third is a deep objective-prism survey in the outer parts of the SMC. As a consequence, any conclusions relating to the rates of evolution across the H-R diagram must be restricted to the brightest objects, log $F_{\mathrm{H}\beta} >$ 13.3 ergs cm^{-2} s^{-1}.

The Magellanic Cloud PNs have been assigned excitation classes by Morgan (1984) of the basis of UK Schmidt objective-prism plates. The classification criteria were based on a combination of those used by Feast (1968) and Webster (1975). These, in turn, are based on the scheme originally developed by Aller (1956), which essentially measures the excitation of the helium ions. The problem with such a classification scheme is that it is divided into discrete steps. The relationship between excitation class and T_{eff} is rather analogous to the relationship between stellar spectral type and T_{eff} in the case of stars. In order to represent the evolution of the "transformed" H-R diagram, the excitation class should be a smooth or fine-grained, rather than a discrete, variable. In order to refine the definition of excitation class, we have used the spectrophotometry of Monk, Barlow, and Clegg (1988) to attempt to find a simple relationship between the principal defining line ratios of the classification scheme and the excitation class, which results in a scheme which agrees closely with the Morgan (1984) classification. The relationships so found are

$$\mathrm{E.C.} = 0.45[F(5007)/F(\mathrm{H}\beta)] \qquad (0.0 < \mathrm{E.C.} < 5.0)\,, \tag{2.1a}$$

$$\mathrm{E.C.} = 5.54[F(4686)/F(\mathrm{H}\beta) + 0.78] \qquad (5.0 \leq \mathrm{E.C.} < 10.0)\,, \tag{2.1b}$$

which give the excitation class as a continuous variable. Note that this definition will imply that in the higher excitation nebulae the excitation classification will be somewhat dependent on the nebular helium abundance. This being the case, a definition which depends on the He I/He II line ratio might have been more logical. These and other line ratios which are sensitive principally to the excitation class are plotted in Figure 1 (derived from the Monk, Barlow, and Clegg 1988 data set). Morgan (1984) has used the [Ne III] line intensity as a secondary criterion for the definition of excitation class in the vicinity of E.C. ~ 4–5. However, Figure 1 shows that this is subject to a fair degree of scatter. As can be seen from Figure 2, the agreement between the excitation class derived here and that given by Morgan (1984) is excellent, especially when the difficulty of measuring line ratios from objective-prism plates is taken into consideration.

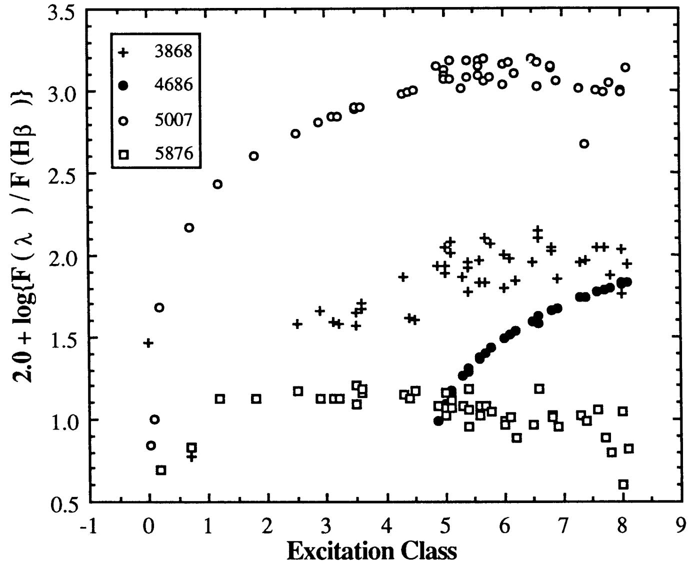

FIG. 1.—Variation of line ratios with respect to Hβ with excitation class for the [O III] λ5007, He II λ4686, [Ne III] λ3868, and He I λ5876 lines, from the Monk, Barlow, and Clegg (1988) sample of objects in the LMC. Our excitation classification depends on the [O III]/Hβ line ratio up to excitation class 5, and on the He II/Hβ ratio thereafter, as described in text.

The nebular densities are derived from the [O II] ratio λ3726/λ3729. These are published in Dopita *et al.* (1988). This is supplemented with data from Barlow (1987) and Monk, Barlow, and Clegg (1988). The nebular fluxes come from Meatheringham, Dopita, and Morgan (1988), supplemented by fluxes given in Wood, Bessell, and Dopita (1986) and Wood *et al.* (1987). From these, nebular masses have been derived using equation (2) of Meatheringham, Dopita, and Morgan (1988), with the additional assumption that the mean logarithmic reddening constant at Hβ is 0.18 for the LMC and 0.1 for the SMC.

For some objects, diameters have been directly determined, either by using speckle interferometry (Wood, Bessell, and

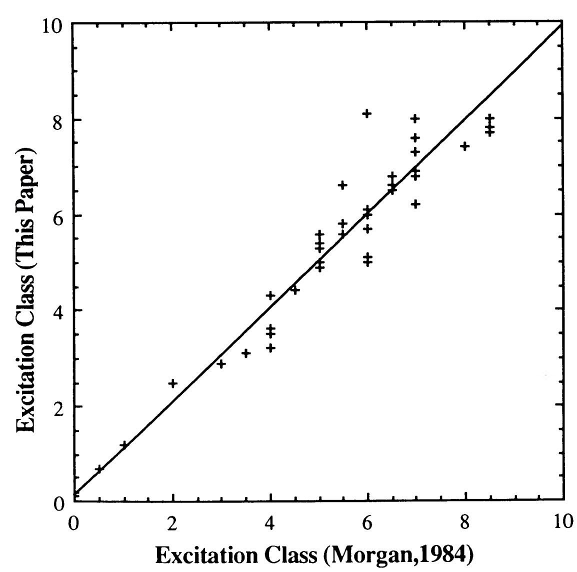

FIG. 2.—Comparison of the Morgan (1984) objective-prism survey excitation classification and our excitation classification of the Monk, Barlow, and Clegg (1988) sample of PNs in the LMC.

1990ApJ...357..140D

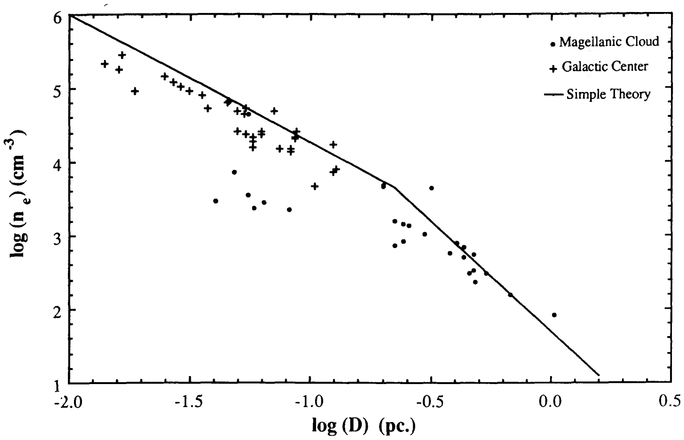

FIG. 3.—Correlation of diameter and density in the Magellanic Cloud and Galactic center PNs. The cluster of Magellanic Cloud points in the vicinity log $D = -1.2$; log $n_e = 3.5$ are derived from speckle interferometry, and, presumably, only the bright cores of the nebulae are detected in this case. The line is derived from the simple theory described in text. For estimated errors on this and other correlations, refer to source references quoted in text.

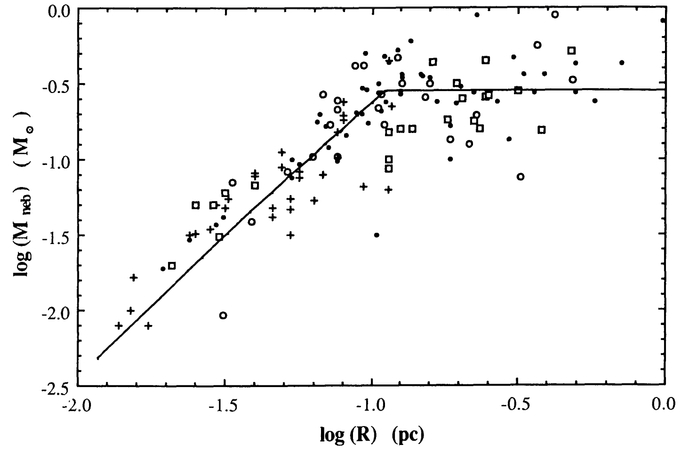

FIG. 5.—Correlation of radius and nebular mass for Magellanic Cloud and Galactic center PNs. Crosses refer to the Galactic center PNs of Gathier *et al.* (1983), and squares to Magellanic Cloud PNs for which the diameter has been directly determined. Open circles and closed circles represent objects in the SMC and LMC, respectively, for which the diameter has been estimated from the density by the correlation of Fig. 3. The line is the fit of the simple theory described in text.

Dopita 1986) or by direct imaging (Wood *et al.* 1987). If this list is supplemented by the observations of Galactic center PNs (Gathier *et al.* 1983), a close relationship between diameter and density emerges (see Fig. 3). In deriving the points on the diagram, the Galactic center points have been derived from equation (1) of Gathier *et al.* (1983), assuming a distance of 8.5 kpc and a filling factor of 0.18, appropriate to their mean diameter (see § III below). For the Magellanic Cloud points with diameters greater than log $D = -0.7$ and log $n_e < 3.0$, the densities are derived from the Hβ fluxes, using a filling factor of 0.38, appropriate for optically thin PNs. Note that the Magellanic Cloud points derived from speckle interferometry generally fall well below the correlation defined by the other points. This is clear evidence that the structures seen in speckle interferometry are dense bright cores (which are presumably weak in [O II]). This is consistent with the fact that the diameters derived from the observed Hβ fluxes and [O II] densities are, in general, larger than those derived from the speckle interferometry (Wood, Bessell, and Dopita 1986).

Figure 3 implies that the observed density can be used to estimate diameters to an accuracy of about ± 0.15 dex for those objects where direct observations do not exist. The observed expansion velocities (Dopita *et al.* 1985, 1988) are used to derive the dynamical ages using the diameters either directly observed or inferred from the density. A correlation which is often used in the confrontation between theory and observation is the relationship between expansion velocity and radius. In practice, this is rather weak both for Magellanic Cloud PNs (Fig. 4) and for Galactic PNs (Sabbabin and Hamzaoglu 1982; Phillips 1984).

There is a much better correlation between nebular mass and radius (Fig. 5). This correlation shows a sharp discontinuity at log $R \sim -0.05$, log $n_e \sim 3.65$. This can be associated with the transition from the optically thick to optically thin stages of evolution (Wood 1987; Barlow 1987; Meatheringham, Dopita, and Morgan 1988).

The correlation between dynamical age and density (Fig. 6) is a clear demonstration that all other correlations represent an

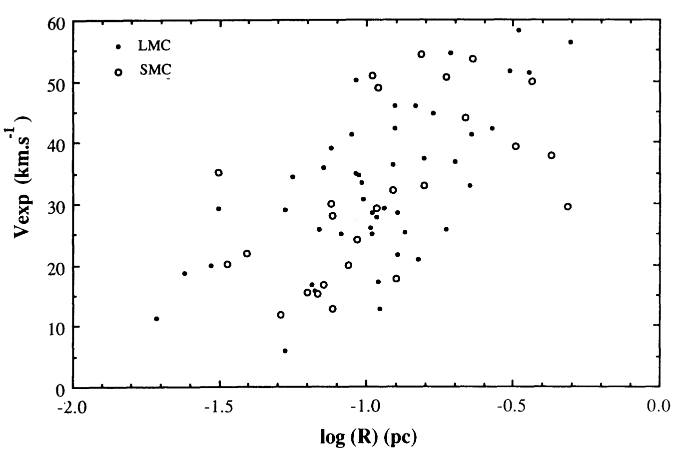

FIG. 4.—(Weak) correlation of expansion velocity and radius for the Magellanic Cloud PNs. Open circles refer to SMC PNs, and closed circles to LMC objects. This correlation is often used to attempt to distinguish between different dynamical models. However, it is clear that it is insensitive for this purpose.

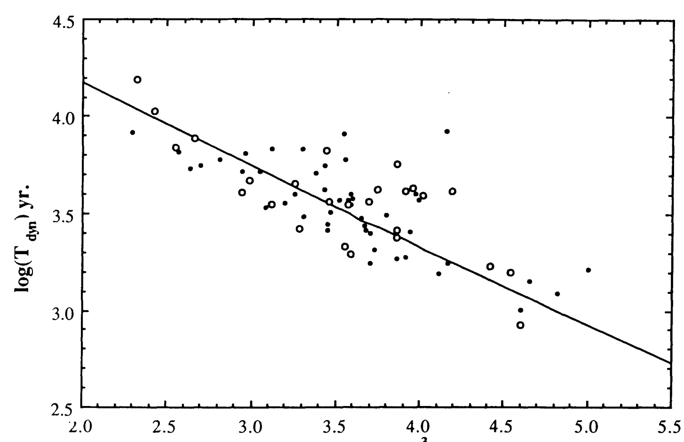

FIG. 6.—Correlation of the dynamic age with density. Symbols and the line have the same meanings as in Fig. 5.

evolutionary sequence of PNs. We will now construct a simple first-order theory which reproduces all these correlations.

III. A FIRST-ORDER EVOLUTIONARY MODEL

Given the complexities of the physics of the coupled evolution of the central star and the nebula touched upon in the introduction, our objective is not to produce a detailed model for the full evolution of PNs, but rather, to provide the simplest semiempirical model that is capable of reproducing the various correlations presented above.

As discussed in Dopita *et al.* (1987), an idealized spherical model of a PN has a complex system of concentric zones, which in the optically thick case consist of the following (in order, working in):

1. The undisturbed and un-ionized AGB wind, bounded by an approximately isothermal shock;
2. A shock-compressed isobaric un-ionized shell, bounded by a weak D-type ionization front;
3. An isobaric H II region, which absorbs all the ionizing photons from the PNN;
4. A contact discontinuity between the H II region and the shock-heated stellar wind;
5. A layer of shock-heated stellar wind gas, bounded by a strong shock;
6. A zone of undisturbed radiatively accelerated stellar wind gas from the PNN;

(see Dyson 1981; Kahn 1983; Kwok and Volk 1985; Volk and Kwok 1985). In the case that the total energy content of zones 2–5 (inclusive) can be represented by a simple power law in time, $E(t) = E_0 t^{\alpha}$, and if the radial density distribution in the undisturbed AGB wind is given by a power law in radius, $\rho(r) = \rho_0 r^{\beta}$, then, from dimensional considerations, the radius of the outer shock, R, is given by

$$R = A(E_0/\rho_0)^{1/(5+\beta)} t^{(2+\alpha)/(5+\beta)} , \tag{3.1}$$

and the velocity of expansion, $V_{\rm exp}$, is given by

$$V_{\rm exp} = B(E_0/\rho_0)^{1/(5+\beta)} t^{(\alpha-\beta-3)/(5+\beta)} , \tag{3.2}$$

with A and B dimensionless constants.

Let us assume that the nebula is evolving into a AGB wind that has been blown at a steady mass-loss rate and velocity. Thus $\beta = -2$. The observational material on the Magellanic Cloud PN therefore limits α to lie in the bounds $1 < \alpha < 2$. This result can be understood on the basis of radiative-driven wind theory where the wind acquires a momentum close to that of the radiation field (L_*/c), and a velocity that is -1.5–3.5 times the escape velocity, $v_{\rm esc}$ (Abbott 1979). The rate of energy input is then given by any of the following:

$$\begin{aligned} dE/dt &= 0.5 v_\infty^2 \partial M_*/\partial t = \phi(L_*/c) v_{\rm esc} \\ &= \phi(L_*/c)(GM_*/2)^{1/2} R_*^{-1/2} \\ &= (\phi/c)(4\pi\sigma)^{1/4}(GM_*)^{1/2} L_*^{3/4} T_{\rm eff} , \end{aligned} \tag{3.3}$$

where ϕ is a constant of order unity, σ is Stefan's constant, and L_*, M_*, R_*, $T_{\rm eff}$ are the luminosity, mass, radius, and effective temperature, respectively, of the central star.

The PNN evolutionary models of Wood and Faulkner (1986) indicate that, for a 0.6 $M_\odot$ model with ejection phase 0.5, dE/dt is approximately constant initially, rises at $\sim t^{0.7}$ between 10^3 and 10^4 yr, and falls precipitately once the maximum of temperature has been passed. In the case of ejection phase 0.0, dE/dt varies as $t^{0.17}$ up to the maximum, before once again declining steeply. Thus, up to the maximum of temperature, α lies in the theoretical range $1 < \alpha < 1.7$, which is similar to the bounds inferred from observation.

Let us distinguish two limiting cases, $\alpha = 1.0$ and $\alpha = 2.0$. These are then characterized by the following expansion velocity/radius relationships:

$$\begin{aligned} &\alpha = 1.0, \quad V_{\rm exp} = {\rm const.}, \qquad R = {\rm const.}\ t ; \\ &\alpha = 2.0, \quad V_{\rm exp} = {\rm const.}\ R^{1/4}, \qquad R = {\rm const.}\ t^{4/3} . \end{aligned} \tag{3.4}$$

The velocity of expansion therefore depends only very weakly on radius, for optically thick evolution, a result supported by observations (Sabbabin and Hamzaoglu 1982; Phillips 1984, see also Fig. 4). The weakness of this dependence makes it a poor test of theoretical evolutionary scenarios, despite its fairly extensive use in the literature (e.g., Sabbadin *et al.* 1984; Okorokov *et al.* 1985).

The stellar wind provides the pressure which confines the ionized material to a thin shell. The pressure of the stellar wind is in equilibrium with the gas pressure in the H II region. Thus, if the inner stellar wind shock occurs at $R_{\rm in} = \theta R$, then

$$P = \phi L_*/4\pi c \theta^2 R^2 = \mu m_{\rm H} n c_{\rm II}^2/3 ,$$

where n is the number density in the H II region with sound speed $c_{\rm II}$. The value of θ is about 0.3 in similarity solutions. Applying simple Strömgren theory to the H II region then yields

$$\Delta R/R = {\rm const.}\ (S_*/\phi^2 L_*^2)\theta^4 R .$$

Thus, in the case $\alpha = 1.0$, where the term in parentheses is constant, this equation gives the following relationship between the thickness of the ionized shell and its radius:

$$R = {\rm const.}\ (\Delta R/R)/(1 - \Delta R/R)^4 . \tag{3.5}$$

In terms of these same parameters, the density is given by

$$n = {\rm const.}\ R^{-3/2}(\Delta R/R)^{-1/2} , \tag{3.6}$$

from which the ionized nebular mass may be computed.

Equations (3.5) and (3.6) represent our simple optically thick sequence. In order to relate it to observations, we need to normalize these to a point of reference. This is taken as the observed transition point between optically thick and optically thin sequence, log $R = -0.95$, log $n_e = 3.65$, log $(M/M_\odot) = -0.55$. These figures then imply $\Delta R/R = 0.16$ at the optically thick-thin transition, which is close to that observed (Phillips 1984). The parameters of the optically thick sequence are given in Table 1.

TABLE 1

ADOPTED NEBULAR PARAMETERS FOR THE OPTICALLY THICK SEQUENCE

Radius (pc)	($\Delta R/R$)	log n (cm^{-3})	log $(M/M_\odot)$
0.0118.....	0.03	5.490	−2.317
0.0214.....	0.04	5.215	−2.045
0.0267.....	0.06	4.809	−1.578
0.0388.....	0.08	4.503	−1.351
0.0530.....	0.10	4.252	−1.108
0.0696.....	0.12	4.035	−0.900
0.0891.....	0.14	3.840	−0.715
0.1118.....	0.16	3.646	−0.547
0.1385.....	0.18	3.498	−0.391

When the nebula becomes optically thin to the ionizing radiation, two limiting cases may be recognized. In the first of these, we assume that the central star has not yet reached its maximum of temperature, so that the luminosity is constant, and the energy content is proportional to time $E(t) = E_0(t/t_0)$. Since the total and nebular mass is constant, this implies

$$\alpha = 1.0\ , \quad V_{\rm exp} = {\rm const.}\ R^{1/3}\ , \quad R = {\rm const.}\ t^{3/2}\ , \quad AR/R = {\rm const.}\ R^{-1}\ . \tag{3.7}$$

On the other hand, if the star has passed its peak of temperature, the energy input falls rapidly. In the limiting case $\dot{E}(t) = 0.0$, this implies

$$\alpha = 0.0\ , \quad V_{\rm exp} = {\rm const.}\ , \quad R = {\rm const.}\ t \quad \Delta R/R = {\rm const.} \tag{3.8}$$

In the case given by equation (3.7), the nebular density falls as R^{-2}, while in the case given by equation (3.8) it falls as R^{-3}. Observationally, the appropriate power seems to fall between these two extremes (Phillips 1984; Meatheringham, Wood, and Faulkner 1988).

Both the optically thick and the optically thin (case $\alpha = 0.0$) sequences are plotted in Figures 5 and 6. A pleasing simulation of the observed evolutionary sequence is obtained, especially bearing in regard the simplicity of the model. The neglect of the mass dependence of stellar mass loss may be the most serious simplification. Note that at the lowest densities, the scatter in nebular mass becomes great. There is a suggestion of a bifurcation into a low-excitation, low-mass sequence, and a high-excitation, high-mass sequence at these lowest densities. It is possible that this is an effect of stellar mass, in which the lowest mass PNN always evolve in an optically thick nebula, since they neither possess a stellar wind capable of rapidly dissipating the nebula, nor photons sufficient to ionize it.

IV. PHOTOIONIZATION MODELS

a) *Details of the Models*

We have used the generalized modeling code MAPPINGS (Binette, Dopita, and Tuohy 1985) to compute the emission-line spectra of isobaric model PNs, taking into account the evolution and true flux distribution of the central stars, the dynamical evolution of the nebula, and the chemical abundances.

The emission-line spectrum of a photoionized nebula depends on the chemical abundances, the photon energy distribution, and the ionization parameter (the number of photons crossing a unit area per unit time divided by the particle density). In the case of H II regions, Evans and Dopita (1985) and Dopita and Evans (1986) showed that the ratio of [O III]/Hβ is sensitive to all of these, which is unfortunate, since it is used as a primary definition of excitation class for PNs. However, the close coupling of the radius and density turns out to be very useful in minimizing the effect of the ionization parameter, at least. For the optically thick $\alpha = 1.0$ sequence, the density varies as $R^{-2.08}$, which is very close to the power-2 which would keep the ionization parameter constant throughout the sequence, with given central star parameters. In the optically thin sequences, the $\alpha = 1.0$ sequence has exactly the R^{-2} density dependence required, while the $\alpha = 0.0$ sequence has an R^{-3} density dependence, which means that the ionization parameter will vary only slowly with radius. Thus, the effect of the ionization parameter is only of second-order importance in PNs.

The nebular abundances adopted are appropriate to the LMC. The sources used are Monk, Barlow, and Clegg (1988) for N, O, Ne, and Ar, which are appropriate to the PNs. In the case of He, an average between the Dopita (1987) and Russell, Bessell, and Dopita (1988) values and the Monk, Barlow, and Clegg (1988) values is taken. The Monk, Barlow, and Clegg (1988) value allows for enhanced values of the collisional excitation rates predicted theoretically. This point is discussed in detail below. For the heavier elements and for C, the values given in the former sources are taken. By number, with respect to H, the abundance set is He:C:N:O:Ne:Mg:Si:Cl:Ar = 0.088:6×10^{-5}:6.5×10^{-5}:3.1×10^{-4}: 4.4×10^{-5}: 1.6×10^{-5}:2.2×10^{-5}: 8×10^{-6}:9×10^{-8}: 8×10^{-7}. Since dredge-up events can change the nebular abundance of C in particular, we also investigated the effect of changing the C abundance to 4.6×10^{-4}; however, this had a negligible effect on the emission-line ratios in the optical part of the spectrum.

Previous photoionization models have generally assumed a black body photon distribution. This may yield an incorrect excitation, particularly when atmospheric blanketing in He$^+$ is important. A problem of using theoretical model atmospheres is that models do not exist for the exact ($T_{\rm eff}$, log g) parameters required for the central stars. The most complete grid of models is that due to Hummer and Mihalas (1970*a*, *b*), which cover the range $30{,}000 \leq T_{\rm eff} \leq 200{,}000$ K and $3.4 \leq \log g \leq 7.5$, and we have used this as the source for our interpolated atmospheres. Fluxes at each of the ionization edges are given (Hummer and Mihalas 1970*b*), and from this the flux discontinuities at each edge and the slopes between edges were determined. From this the flux distributions at the particular ($T_{\rm eff}$, log g) parameters required were derived by linear interpolation between the nearest models. Figure 7 gives an example of such a synthetic model atmosphere.

Hydrostatic evolutionary sequences for 0.6 and 0.7 $M_\odot$ PNN were taken from Wood and Faulkner (1986). The case of ejection occurring midway between helium shell flashes (phase, $\phi = 0.5$) and during rising luminosity during a flash ($\phi = 0.0$) were both considered. Their case A mass loss was adopted, since this is more consistent with radiatively driven mass-loss theory.

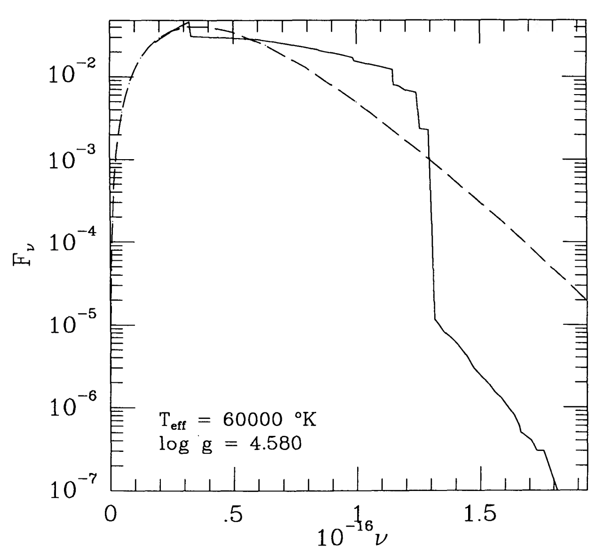

FIG. 7.—Example of a synthetic stellar model atmosphere computed using the interpolation procedure derived in text.

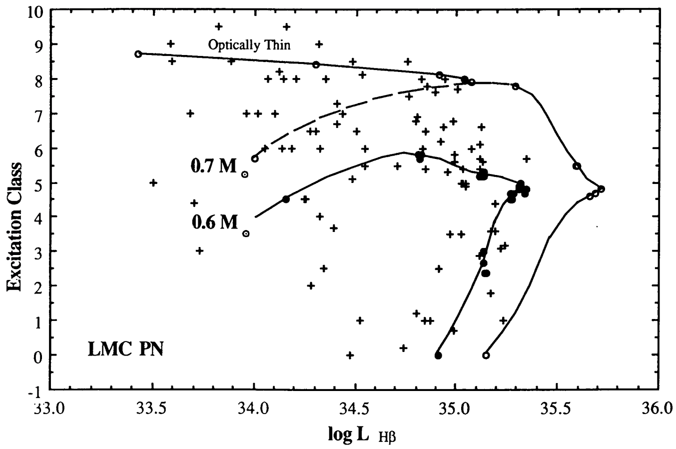

FIG. 8.—Transformed H-R diagram for the LMC PNs (*crosses*). Theoretical tracks for optically thick evolution are shown. Clusters of points on each evolutionary track represent the effect of moving along the nebular evolutionary sequence, from a density of 50,000 cm^{-3} to a density of 5000 cm^{-3}. The results are therefore fairly independent of nebular density. For the 0.7 $M_{\odot}$ track, the effect of making the model which has the highest stellar effective temperature progressively optically thin is also shown. The régime of high excitation and low Hβ flux is therefore populated by optically thin PNs with high-mass central stars.

It is not necessary to compute time-dependent photoionization, as was done by Tylenda (1983, 1986), although MAPPINGS has this facility. Conditions close to photoionization equilibrium are reached in a time scale equal to the recombination time scale in an H II region. This time scale is, approximately, $t_{\rm rec} \sim (10^5/n)$ yr, where the particle density n is measured in cm^{-3}. For the Magellanic Cloud sample, this ratio is always less than 0.1, so nonequilibrium effects are negligible.

Most of the flux from the central star is released as H-ionizing photons. In an optically thick nebula in photoionization equilibrium, each ionization is matched by a recombination in the nebula. Since a fixed fraction of these give rise to an Hβ photon, the flux in this line will be closely related to the luminosity of the central star. Since the excitation class is closely related to Zanstra temperature, then an appropriate transformation of the H-R diagram to observable nebular parameters is to replace luminosity by Hβ flux and temperature by excitation class. In Figures 8 and 9 we plot the transformed H-R diagram for the LMC and SMC sample,

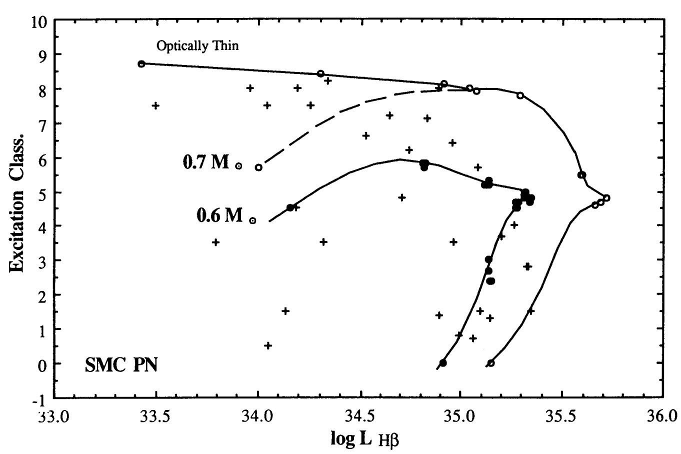

FIG. 9.—As in Fig. 8, but for the SMC

respectively. Distances of 50 and 62 kpc are assumed, and mean intrinsic reddenings of 0.19 and 0.1 dex at Hβ are assumed for the LMC and the SMC, respectively. The evolutionary tracks for stellar evolution ($\phi = 0.5$; case A mass loss) in an optically thick nebula of inner radius 1.9×10^{17} cm and density 10^4 cm^{-3} are shown. Each cluster of points about these tracks shows the effects of moving along the evolutionary sequence from a density of 5×10^3 cm^{-3} to a density of 5×10^5 cm^{-3}. Note that this makes very little difference to either the flux or the excitation class. This is a fortuitous consequence of the fact that the nebular density varies almost as R^{-2} along the nebular evolutionary sequence. For the 0.7 $M_{\odot}$ evolutionary sequence, we have also plotted the trajectory followed by optically thin models, assuming the nebula becomes optically thin at the maximum of stellar temperature.

The curious tongue in both evolutionary curves near excitation class 5 is a consequence of atmospheric blanketing by the He$^+$ ion in the temperature range log $T_{\rm eff} \sim 4.8$–5.1. In this range, the excitation class is very insensitive to temperature, so that we can think of the transformed H-R diagram as being "pinched up" in this region. It is not clear how real this feature may be. Certainly, the observed points show no tendency to cluster in this region, so this feature may simply be an artifact of the LTE stellar atmospheric models used.

b) The Mass Distribution of PNN

For low excitation classes, it is evident that the distribution of points in Hβ flux is closely related to the distribution of masses of the central stars. This is because the luminosity of the central star is related to its mass in this portion of the H-R diagram by the relationship

$$L/L_{\odot} = 59250(M/M_{\odot} - 0.495) \qquad (4.1)$$

(Wood and Zarro 1981), and the high temperature of the central star ensures that, for the optically thick sequence, the Hβ luminosity is closely coupled to the luminosity. If we adopt the optically thick assumption, which is probably valid for excitation classes less than ~ 3, then any mass estimates based on the Hβ luminosity are directly coupled to uncertainties in the apparent distance modulus of the Clouds. For the LMC, the highest mass PNN seems to be $\sim 0.7\ M_{\odot}$, the average mass is close to 0.6 $M_{\odot}$, and since the minimum Hβ is approximately 0.2 dex below the 0.6 $M_{\odot}$ track, we can conclude from equation (4.1) that the minimum mass PNN is near 0.56 $M_{\odot}$. For the SMC, the total range in mass seems to be very similar, but the mean mass may be somewhat higher, $\sim 0.63\ M_{\odot}$. It is difficult, on the basis of the few points available to us in the appropriate range of excitation class (approx. 0–3), to draw firm conclusions on the true distribution of masses of the PNN. However, it is certainly true that a correction for the rate of evolution across the transformed H-R diagram would tend to push the mean masses higher.

In spite of this, this mean mass is somewhat higher and the mass range wider than the corresponding figures derived by Schönberner (1981). He found, for a group of nearby, old, and evolved PNN that the mean mass was 0.58 $M_{\odot}$ and 85% of objects had masses in the range $\pm 0.03\ M_{\odot}$ about this. This difference may be due to two effects. First, the LMC and SMC stellar populations are systematically younger than that of our solar neighborhood. Second, the rapidity of evolution and faintness of the central star against the nebular continuum militates against the detection and inclusion of high-mass PNN in the Schönberner sample.

The fact that the 0.7 $M_{\odot}$ track evolves to higher luminosities than the observed upper luminosity envelope suggests that PNs with high-mass nuclei very rapidly become optically thin, at least in some directions. However, the evolution through the luminous phase is very rapid, so it is possible that our sample is simply too small to observe these rare, luminous, intermediate excitation PNs. Incidentally, both of these effects lead to the very sharp upper luminosity cutoff Hβ observed. This cutoff should prove a very important tool in the use of PNs as standard candles, a work that has already been commenced by Jacoby and coworkers (Jacoby 1989; Ciardullo *et al.* 1989). Given the rapidity of evolution toward higher excitation class, the more massive objects will tend to be found as faint, optically thin, high-excitation PNs. This conclusion is supported by our spectrophotometry (in preparation) which shows a much larger population of Peimbert type I PNs among this sample.

c) The Acceleration of PN Shells

Dopita *et al.* (1987) had remarked upon the correlation of the velocity of expansion with both of the Hβ luminosity and the excitation class, i.e., with the position of the PNs on your transformed H-R diagram. Given the data available to us now, we have reanalyzed this correlation and find that the best fit occurs for the following parameters:

$$v_{\mathrm{exp}} = 5.83[\mathrm{E.C.} - 1.3(\log L_{\mathrm{H}\beta} - 35.15)]\ \mathrm{km\ s^{-1}}\ . \quad (4.2)$$

In Figure 10 we plot the observed data points, the evolutionary tracks, and the lines of constant velocity of expansion according to this correlation. From this it is difficult to avoid the following conclusions:

First, that PNs with both high- and low-mass PNN undergo an acceleration phase as the central star evolves toward higher temperature, but that the PNs with more massive central stars are accelerated more rapidly.

Second, that PNs with low-mass nuclei probably remain optically thick as the central star fades, and the PN shell is not appreciably accelerated during this phase.

Third, that PNs with high-mass nuclei rapidly become optically thin and continue to be accelerated as the central star fades.

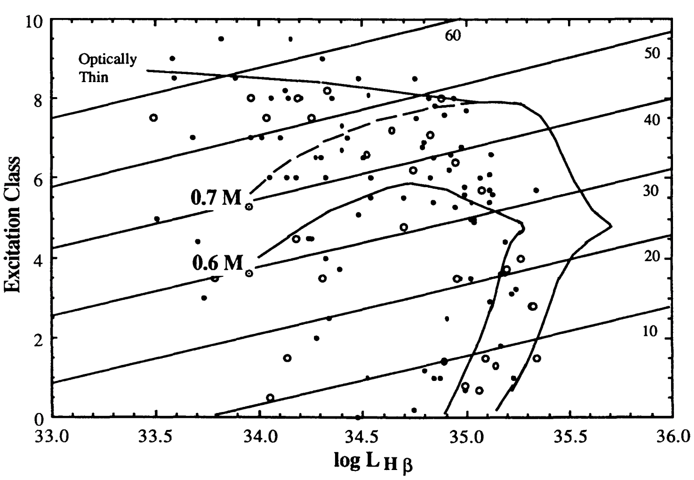

FIG. 10.—Combined LMC and SMC data (*closed and open circles*, respectively) plotted on the transformed H-R diagram. Computed evolutionary tracks are also shown, as are best fit lines of constant expansion velocity. It is clear that the nebulae are accelerated while young, but fade at almost constant expansion velocity.

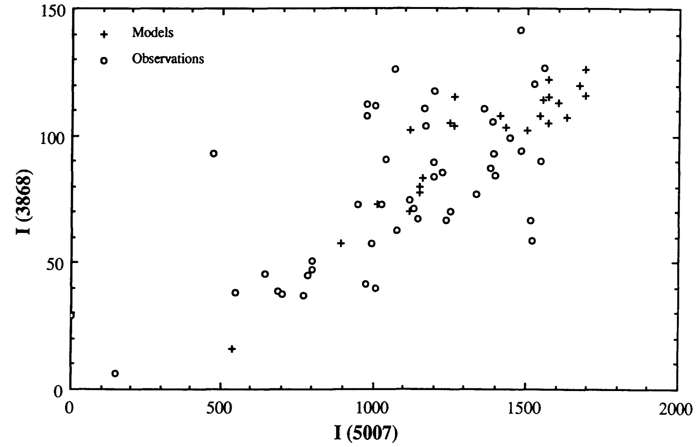

FIG. 11.—Correlation of [O III] λ5007 and [Ne III] λ3868 line flux ratios with Hβ. Open circles refer to the Monk, Barlow, and Clegg (1988) spectrophotometry for the LMC, and crosses are the results from individual photoionization models. There is no systematic offset between these two sets of data.

These results are not in contradiction with the simple model presented in § III above. However, the different evolutionary scenarios implied in Figure 10 for PNs with low- and high-mass central stars implies that much of the scatter in Figures 4–6 may be mass related. This emphasizes the importance of refining this simple model by means of a fully self-consistent evolutionary model for the central star, its stellar wind, and for the ionization and dynamics of the surrounding nebula.

d) Line Ratios and Chemical Abundances

The results of the photoionization models presented so far have used only the Hβ flux, and the definition of excitation class given by equations (2.1a) and (2.1b). How well do the models work in reproducing the secondary line ratios which define excitation class (see Fig. 1)?

First, consider the [Ne III] line at λ3968 Å. In Figure 11, we present the correlation of the [O III] and the [Ne III] line intensities with respect to Hβ for the Monk, Barlow, and Clegg (1988) data, and we compare this with the results of the individual photoionization models. The slopes of the correlations are identical within the errors of measurement. This demonstrates that the models are correctly predicting the relative [Ne III] line intensities for a given excitation class as defined by the [O III]/Hβ ratio, and that therefore the adopted value of the Ne/O ratio, 0.178 by mass, was about correct. This figure is slightly smaller than the value of 0.21 ± 0.06 derived by Henry (1989*a*, *b*), but this small difference is well within the error resulting from the different analysis techniques. Although, in our analysis, we make no attempt to derive the absolute abundances of either element, it is clear that the elemental abundance ratio varies little from object to object within the LMC, which also is in accord with Henry's (1989*a*, *b*) results.

Second, consider the He I λ5876 line. Figure 1 shows that this is well correlated with excitation class, as it should be, since the concept of excitation class is based on helium excitation. Up to about excitation class 2.5, it rapidly increases in relative strength, before declining slowly at higher excitation classes. In Figure 12, we investigate the variation in the He I λ5876/Hβ line ratio as a function of helium abundance and of excitation class. Note that these parameters are coupled above excitation class 5, since the excitation class as defined by the He II λ4686/Hβ ratio depends on the helium abundance as

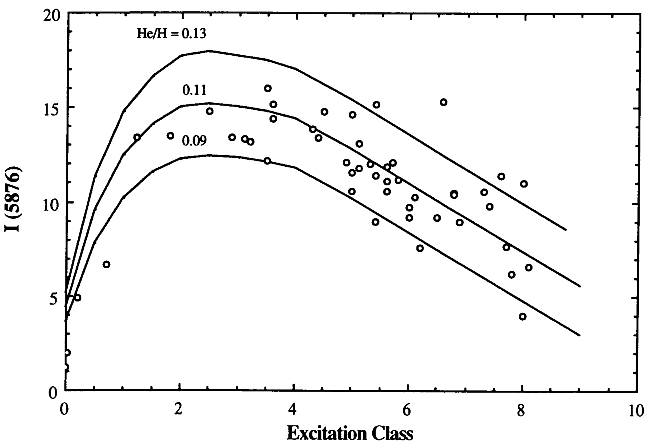

FIG. 12.—Comparison of the He I $\lambda5876/H\beta$ flux ratio and excitation class for models of different He abundance, as described in the text, and the Monk, Barlow, and Clegg (1988) spectrophotometry for the LMC (*open circles*).

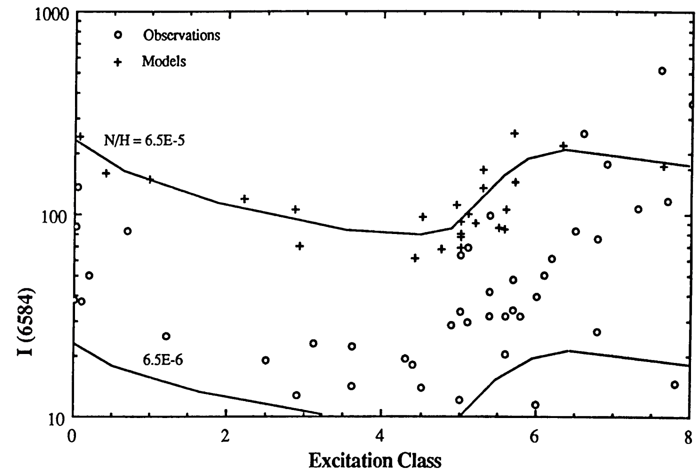

FIG. 13.—Comparison of the [N II] $\lambda6584/H\beta$ flux ratio and the excitation class for models of different N abundance. Crosses indicate the degree of scatter about the mean ratios, plotted as solid lines. Open circles refer to the Monk, Barlow, and Clegg (1988) spectrophotometry for the LMC PNs. Highest excitation objects appear to show real N excess, on average.

well. It is clear that the models reproduce the general trend of the He I $\lambda5876/H\beta$ line ratio rather well. However, it is clear that the mean helium abundance implied is somewhat higher than the value of 0.088 by number adopted originally, and that some of the highest excitation objects appear to show a distinct helium excess.

The difference between the abundances estimated here and those derived by Monk, Barlow, and Clegg (1988) results from the neglect of the collisional contributions to the line from the metastable He I 2 ^3S level in our calculations. The exact magnitude of this effect has remained somewhat uncertain, since this level can be depopulated by collisional ionizations and photoionizations, as well as by collisional excitations to other levels. This problem has recently been addressed by Clegg and Harrington (1989). They find that, at stellar temperatures typical of PNN, the contribution of collisions to the line intensity is $\sim 10\%$ compared with the contribution of recombinations. This nicely accounts for the difference in the derived mean abundances. However, the scatter among the high-excitation objects appears to be real, and the derived abundances for the objects with the largest He I line intensities are larger than could be accounted for by collisional enhancement. We therefore conclude that we are seeing real helium enhancements in these nebulae, which are mostly classified as Peimbert type I objects with strong nitrogen lines.

Do the strong nitrogen lines in these objects in fact imply overabundances of nitrogen? In Figure 13, we plot the theoretical run of the [N II] $\lambda6584/H\beta$ line ratio with N abundance and excitation class. Such a diagram is particularly useful in PN nebular abundance diagnostics, since the ionization correction factors are included implicitly, as in any change in temperature of the zone of the nebulae containing N^+ resulting from changing $T_{\rm eff}$ of the central star. The Monk, Barlow, and Clegg (1988) points fall along a line of constant abundance up to about excitation class 6, above which there is a clear tendency for N abundance to rise with increasing excitation class. This cannot be due to the optically thick-thin transition, since the highest excitation objects are expected to be optically thin, in which case the [N II] lines would tend to weaken, rather than strengthen. We conclude that there are real enhancements in the N abundance in high-excitation type I nebulae.

Both carbon and nitrogen are produced largely in intermediate-mass stars during three convective dredge-up episodes (Iben 1975; Iben and Truran 1978; Renzini and Voli 1981). During the first of these, ^{14}N is enhanced at the expense of ^{12}C. In the second phase, the so-called hot-bottom burning phase is initiated following the ignition of the He and occurs in stars more massive than 3–5 $M_\odot$. The result is also to dredge up nitrogen and helium. The third phase occurs during AGB evolution and is a result of the helium shell flashes, which turn off the hydrogen burning and allow the convective zone to penetrate all the way into the intershell region where incomplete helium burning has occurred. Correspondingly, each shell flash allows significant amounts of ^4He and ^{12}C to reach the surface. On the basis of this, we would expect that hot-bottom burning would result in correlated helium and nitrogen enhancements, as has been observed to be the case in Galactic PNs (Kaler 1978, 1980). In Figure 14 we show the abundances derived for these elements using Figures 12 and 13. There is, indeed, a correlation between the N and He enhancements. This proves that hot-bottom burning does in fact take place in

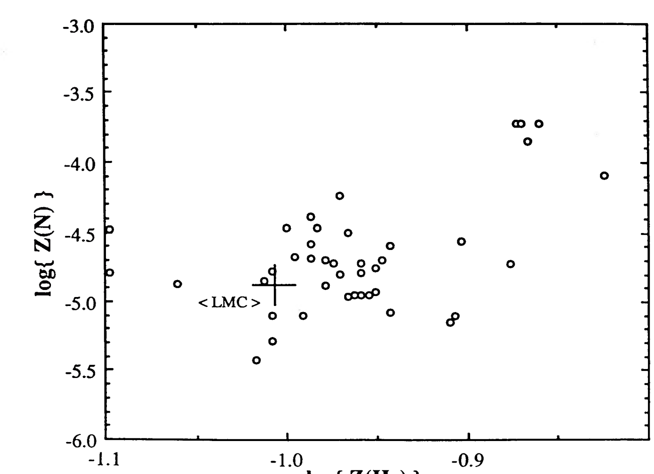

FIG. 14.—Comparison of the N and He abundances derived from Figs. 13 and 14. There are correlated abundance enhancements, proving that dredge-up and ejection of H-burnt products has occurred.

the Magellanic Cloud PNs; however, the N excesses are not as large, at given He/H ratio, as for the Galactic PNs.

Since the dredge-up processes are expected to produce strong enhancements of ^{12}C, we have run models with high carbon abundance, as high as 4.6×10^{-4} by number; i.e., a C/O ratio of 1.5. Curiously, this seems to have a negligible effect on either the excitation class or the emission-line ratios.

V. CONCLUSIONS

We have been able to show that the optically thick PNs in the Magellanic Clouds behave as ram-pressure confined H II regions, trapped between the shocked remnants of AGB wind and the high-velocity stellar wind of the PNN. This has allowed us both to calculate their dynamical evolution and their spectral evolution on a transformed H-R diagram.

While this theory is certainly capable of giving an overall phemenological description, it is only a first-order model. We intend to refine it by performing a fully self-consistent evolutionary computation. This will involve the computation of the evolution of the central star, and, by applying the recently refined radiatively driven stellar mass-loss theory of Kudritski and his coworkers (Kudritski, Pauldrach, and Puls 1987), we will be able to derive explicitly the dynamical evolution of the PN. Detailed photoionization modeling can then be applied to the ionized nebula to compute the abundances of the various elements. Since we expect to have available both imaging and UV spectrophotometry obtained with the Hubble telescope, we may expect this approach to furnish new insight and strong observational constraints into planetary nebula evolution, chemical dredge-up, and the giant wind mass ejection processes.

REFERENCES

Abbot, D. C. 1978, *Ap. J.*, **225**, 893.
Aller, L. H. 1956, *Gaseous Nebulae* (New York: Wiley).
Barlow, M. J. 1987, *M.N.R.A.S.*, **227**, 161.
Binette, L., Dopita, M. A., and Tuohy, I. R. 1985, *Ap. J.*, **297**, 476.
Ciardullo, R., Jacoby, G. H., Ford, H. C., and Neil, J. D. 1989, *Ap. J.*, **339**, 53.
Clegg, R. E. S., and Harrington, J. P. 1989, *M.N.R.A.S.*, **239**, 869.
Clegg, R. E. S., Harrington, J. P., Barlow, M. J., and Walsh, J. R. 1986, *Ap. J.*, **314**, 551.
Dopita, M. A. 1987, in *IAU Symposium 115, Star-forming Regions*, ed. M. Peimbert and J. Jugaku (Dordrecht: Reidel), p. 501.
Dopita, M. A., and Evans, I. N. 1986, *Ap. J.*, **307**, 431.
Dopita, M. A., Ford, H. C., Lawrence, C. J., and Webster, B. L. 1985, *Ap. J.*, **296**, 390.
Dopita, M. A., Ford, H. C., and Webster, B. L. 1985, *Ap. J.*, **297**, 593.
Dopita, M. A., Meatheringham, S. J., Webster, B. L., and Ford, H. C. 1988, *Ap. J.*, **327**, 639.
Dopita, M. A., Meatheringham, S. J., Wood, P. R., Ford, H. C., Webster, B. L., and Morgan, D. H. 1987, *Ap. J. (Letters)*, **315**, L107.
Dyson, J. E. 1981, in *Investigating the Universe*, ed. F. D. Kahn (Dordrecht: Reidel), p. 125.
Evans, I. N., and Dopita, M. A. 1985, *Ap. J. Suppl.*, **58**, 125.
Feast, M. W. 1968, *M.N.R.A.S.*, **140**, 345.
Gathier, R., Pottasch, S. R., Goss, W. M., and van Gorkom, J. M. 1983, *Astr. Ap.*, **128**, 325.
Härm, R., and Schwartzschild, M. 1975, *Ap. J.*, **200**, 324.
Harman, R. J., and Seaton, M. J. 1964, *Ap. J.*, **140**, 824.
Harrington, J. P., Seaton, M. J., Adams, S., and Lutz, J. H. 1982, *M.N.R.A.S.*, **199**, 517.
Henry, R. B. C. 1989*a*, *Rev. Mexicanà Astr. Ap.*, in press.
———. 1989*b*, *M.N.R.A.S.*, **241**, 453.
Hummer, D. G., and Mihalas, D. 1970*a*, *M.N.R.A.S.*, **147**, 339.
———. 1970*b*, *JILA Rept.*, No. 101, University of Colorado.
Iben, I., Jr. 1984, *Ap. J.*, **277**, 333.
———. 1975, *Ap. J.*, **196**, 525.
Iben, I., Jr., and Truran, J. W. 1978, *Ap. J.*, **220**, 980.
Jacoby, G. H. 1980, *Ap. J. Suppl.*, **42**, 1.
———. 1989, *Ap. J.*, **339**, 34.
Kahn, F. D. 1983, in *IAU Symposium 103, Planetary Nebulae*, ed. D. R. Flower (Dordrecht: Reidel), p. 305.
Kaler, J. B. 1978, *Ap. J.*, **226**, 946.
———. 1980, *Ap. J.*, **239**, 592.
Kudritski, R. P., Pauldrach, A., and Puls, J. 1987, *Astr. Ap.*, **173**, 293.
Kwok, S. 1982, *Ap. J.*, **258**, 280.
Kwok, S., Purton, C. R., and Fitzgerald, P. M. 1978, *Ap. J. (Letters)*, **219**, L125.
Kwok, S., and Volk, K. 1985, *Ap. J.*, **299**, 191.
Mathews, W. G. 1966, *Ap. J.*, **143**, 173.
Meatheringham, S. J., Dopita, M. A., Ford, H. C., and Webster, B. L. 1988, *Ap. J.*, **327**, 651.
Meatheringham, S. J., Dopita, M. A., and Morgan, D. H. 1988, *Ap. J.*, **329**, 166.
Meatheringham, S. J., Wood, P. R., and Faulkner, D. J. 1988, *Ap. J.*, **334**, 862.
Monk, D. J., Barlow, M. J., and Clegg, R. E. S. 1988, *M.N.R.A.S.*, **234**, 583.
Morgan, D. H. 1984, *M.N.R.A.S.*, **208**, 633.
Morgan, D. H., and Good, A. R. 1985, *M.N.R.A.S.*, **213**, 491.
O'Dell, C. R. 1974, in *IAU Symposium 66, Late Stages of Stellar Evolution*, ed. R. J. Tayler and J. E. Hesser (Dordrecht: Reidel), p. 213.
Okorokov, V. A., Shustov, B. M., Tutukov, A. V., and Yorke, H. W. 1985, *Astr. Ap.*, **142**, 441.
Paczyński, B. 1971, *Acta. Astr.*, **21**, 417.
Phillips, J. P. 1984, *Astr. Ap.*, **137**, 92.
Pottasch, S. R. 1984, *Planetary Nebulae* (Dordrecht: Reidel).
Renzini, A., and Voli, M. 1981, *Astr. Ap.*, **94**, 175.
Russell, S. C., Bessell, M. S., and Dopita, M. A. 1988, in *IAU Symposium 132, The Impact of Very High S/N Spectroscopy on Stellar Physics*, ed. G. Cayrel de Strobel and M. Spite (Dordrecht: Reidel), p. 545.
Sabbadin, F. 1986, *Astr. Ap.*, **160**, 31.
Sabbadin, F., Gratton, R. G., Bianchini, A., and Ortolani, S. 1984, *Astr. Ap.*, **136**, 181.
Sabbabin, F., and Hamzaoglu, E., 1982, *Astr. Ap.*, **110**, 105.
Sanduleak, N., MacConnell, D. J., and Philip, A. G. D. 1978, *Pub. A.S.P.*, **90**, 621.
Schmidt-Voigt, M., and Köppen, J. 1987*a*, *Astr. Ap.*, **174**, 211.
———. 1987*b*, *Astr. Ap.*, **174**, 223.
Schönberner, D. 1979, *Astr. Ap.*, **79**, 108.
———. 1981, *Astr. Ap.*, **103**, 119.
———. 1983, *Ap. J.*, **272**, 708.
Sofia, S., and Hunter, J. H. 1968, *Ap. J.*, **152**, 405.
Stasinska, G. 1989, *Astr. Ap.*, in press.
Tylenda, R. 1983, *Astr. Ap.*, **126**, 299.
———. 1986, *Astr. Ap.*, **152**, 217.
Vil'koviskii, É. Ya., Kondat'eva, L. N., and Tambovtseva, L. V. 1983, *Soviet Astr.*, **27**, 194.
Volk, K., and Kwok, S. 1985, *Astr. Ap.*, **153**, 79.
Webster, B. L. 1975, *M.N.R.A.S.*, **173**, 437.
Wood, P. R. 1987, in *Late Stages of Stellar Evolution*, ed. S. Kwok and S. R. Pottasch (Dordrecht: Reidel), p. 197.
Wood, P. R., Bessell, M. S., and Dopita, M. A. 1986, *Ap. J.*, **311**, 632.
Wood, P. R., and Cahn, J. H. 1977, *Ap. J.*, **211**, 499.
Wood, P. R., and Faulkner, D. J. 1986, *Ap. J.*, **307**, 659.
Wood, P. R., Meatheringham, S. J., Dopita, M. A., and Morgan, D. H. 1987, *Ap. J.*, **320**, 178.
Wood, P. R., and Zarro, D. M. 1981, *Ap. J.*, **247**, 247.

MICHAEL A. DOPITA: Mount Stromlo and Siding Spring Observatories, Private Bag, Woden P.O., ACT 2606, Australia

STEPHEN J. MEATHERINGHAM: Laboratory for Astronomy and Solar Physics, NASA Goddard Space Flight Center, Code 685, Greenbelt, MD 20771